ACS OMEGA

Open Access

http://pubs.acs.org/journal/acsodf

Article

Photoluminescence of MoS_2 on Plasmonic Gold Nanoparticles Depending on the Aggregate Size

Kiin Nam, Jaeseung Im, Gang Hee Han, Jin Young Park, Hyuntae Kim, Sungho Park, Sungjae Yoo, MohammadNavid Haddadnezhad, Jae Sung Ahn, Kyoung-Duck Park, and Soobong Choi*

Cite This: *ACS Omega* 2024, 9, 21587−21594

Read Online

ACCESS | Metrics & More | Article Recommendations | Supporting Information

ABSTRACT: Transition metal dichalcogenides (TMDs) are promising candidates for ultrathin functional semiconductor devices. In particular, incorporating plasmonic nanoparticles into TMD-based devices enhances the light−matter interaction for increased absorption efficiency and enables control of device performance such as electronic, electrical, and optical properties. In this heterohybrid structure, manipulating the number of TMD layers and the aggregate size of plasmonic nanoparticles is a straightforward approach to tailoring device performance. In this study, we use photoluminescence (PL) spectroscopy, which is a commonly employed technique for monitoring device performance, to analyze the changes in electronic and optical properties depending on the number of MoS_2 layers and the size of the gold nanoparticle (AuNP) aggregate under nonresonant and resonant excitation conditions. The PL intensity in monolayer MoS_2/AuNPs increases as the size of aggregates increases irrespective of the excitation conditions. The strain induced by AuNPs causes a red shift, but as the aggregates grow larger, the effect of p-doping increases and the blue shift becomes prominent. In multilayer MoS_2/AuNPs, quenched PL intensity is observed under nonresonant excitation, while enhancement is noted under resonant excitation, which is mainly contributed by p-doping and LSPR, respectively. Remarkably, the alteration in the spectral shape due to resonant excitation is evident solely in small aggregates of AuNPs across all layers.

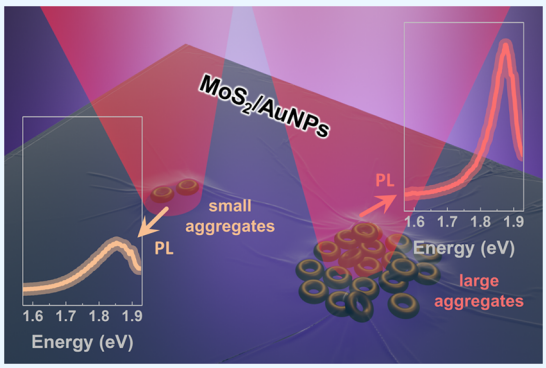

INTRODUCTION

Two-dimensional (2D) semiconducting materials have unique quantum physical properties, such as large exciton binding energy and a direct electronic band gap, owing to their atomically thin molecular structure. Hence, these materials allow us to design functional quantum electronic and photonic devices with ultrathin thickness. Specifically, 2D transition metal dichalcogenides (TMDs) exhibit extraordinary electronic, optical, and mechanical properties, making them primarily employed in optoelectronic and photonic device applications.[1−3]

However, 2D TMDs have relatively low absorption efficiency due to their thin thickness, which limits the generation of photoexcited carriers. Since the resulting low photocurrent and photoluminescence (PL) restrict the overall performance of the device, the practical application of TMDs is inefficient. As a promising strategy for reducing absorption loss, combining TMDs with nanophotonic devices, such as meta-[4−9] and plasmonic[10−17] structures, has garnered significant attention. The heterohybrid structures have the potential to offer new functionalities and exploit synergistic effects through material interactions, which can highly improve the device performance and control the optical, electronic, and electrical properties.

2D TMDs integrated with plasmonic nanoparticles are one of the most beneficial heterohybrid structures.[14−17] The plasmonic nanoparticles contribute to the control of device performance by enhancing the absorption efficiency through plasmonic light−matter interactions and providing additional charge channels and local strain. By placing nanoparticles underneath the 2D TMDs, it becomes feasible to induce the strain. The magnitude and direction of the strain applied to them can be regulated by exercising control over the size, shape, and arrangement of the nanoparticles. The induced strain to 2D TMDs leads to alternations in the crystal lattice with modified interatomic interactions, which give rise to the changed electronic and optical properties.[18−21] Furthermore, plasmonic nanoparticles can also change the electrical properties of adjacent materials at contact interfaces. The band alignment that arises during contact introduces changes in the charge transport behavior and the redistribution of the

Received: March 13, 2024
Revised: April 4, 2024
Accepted: April 22, 2024
Published: April 29, 2024

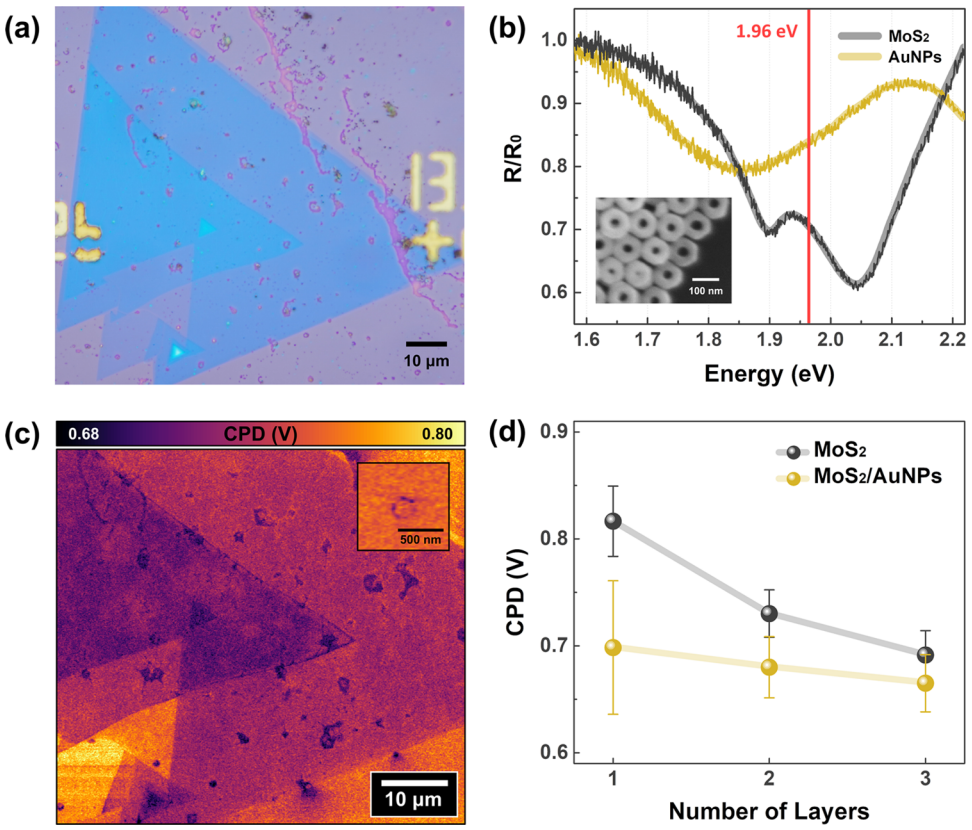

Figure 1. Characterization of the MoS_2/AuNPs hybrid structure. (a) Optical image of MoS_2/AuNPs on the SiO_2/Si substrate. (b) Relative reflectance spectra of MoS_2 and AuNPs. The inset shows the SEM image of AuNPs. (c) Contact potential difference (CPD) image of MoS_2/AuNPs. The inset shows the CPD image of single AuNPs. (d) Layer-dependent CPD of MoS_2 and MoS_2/AuNPs.

electric charge within the system.[22−25] In addition, under resonant optical excitation, the interaction between photons and plasmonic nanoparticles gives rise to a localized surface plasmon resonance (LSPR) effect. This plasmonic excitation is accompanied by nonradiative energy transfer processes such as hot energy transfer and plasmon resonant energy transfer, which enhance carrier generation and plasmonic field.[26−28]

Recently, several reports on heterohybrid-structured devices have attracted attention, in which TMDs are integrated with plasmonic nanoparticles. In these studies, the design and characterization processes play pivotal roles in optimizing the device and improving our understanding of materials by controlling and evaluating their performance. In the design step, modifying the material or shape of device components is a widely used approach to fabricate devices with the desired performance by leveraging alterations in electrical and optical responses resulting from changes in their physical properties.[29−33] However, while adjusting the layer number of TMDs and the aggregate size of nanoparticles is another straightforward approach to control their properties, there is still a lack of studies due to the intricate nature associated with interactions between layers or particles. In the characterization step, PL spectroscopy is useful for analyzing changes in electronic structures caused by local strain and electrical doping and is, therefore, one of the most adopted analysis methods.[18,19,23−25] Especially in plasmonic heterohybrid structures, device performance varies depending on the interaction between the plasmonic nanoparticle and light, so the energy of the excitation light is a crucial controlling factor. Therefore, comparing the PL response under nonresonant and resonant conditions offers additional analytical insights for a better understanding and utilization of the impact of LSPR on device performance.

In this work, we investigated the optical properties of monolayer (1L), bilayer (2L), and trilayer (3L) MoS_2 on both small (<5 particles) and large (>40 particles) aggregates of plasmonic gold nanoparticles (AuNPs); see the Supporting Information, Figure S1. To characterize the optical response of this heterohybrid structure, we measured PL spectra in the energy range of 1.57−1.93 eV using excitation lasers with energies of 1.96 eV (resonance) and 2.33 eV (nonresonance). The PL intensity in 1L MoS_2/AuNPs increases with a higher concentration of AuNPs, regardless of the excitation energy. This trend holds valid for 2L and 3L MoS_2/AuNPs under resonant excitation conditions. Conversely, the PL spectra in 2L and 3L MoS_2/AuNPs exhibit more prominent quenching at larger aggregates of AuNPs under nonresonant excitation conditions. Differences in the spectral shape due to excitation conditions are observed only in MoS_2 on small aggregates of AuNPs. Under resonant excitation conditions, it becomes broader due to the excitonic emission of higher order charge complexes such as trions and biexcitons with lower energies.

RESULTS AND DISCUSSION

Optical and Electrical Characterization of MoS_2/AuNP Heterohybrid Structures. Figure 1a displays the color optical image of the MoS_2/AuNP heterohybrid structures on the SiO_2/Si substrate. As the number of MoS_2 layers increases, the reflection of red light decreases, allowing for the distinction between 1L, 2L, and 3L MoS_2 through changes in the color.

https://doi.org/10.1021/acsomega.4c02442
ACS Omega 2024, 9, 21587−21594

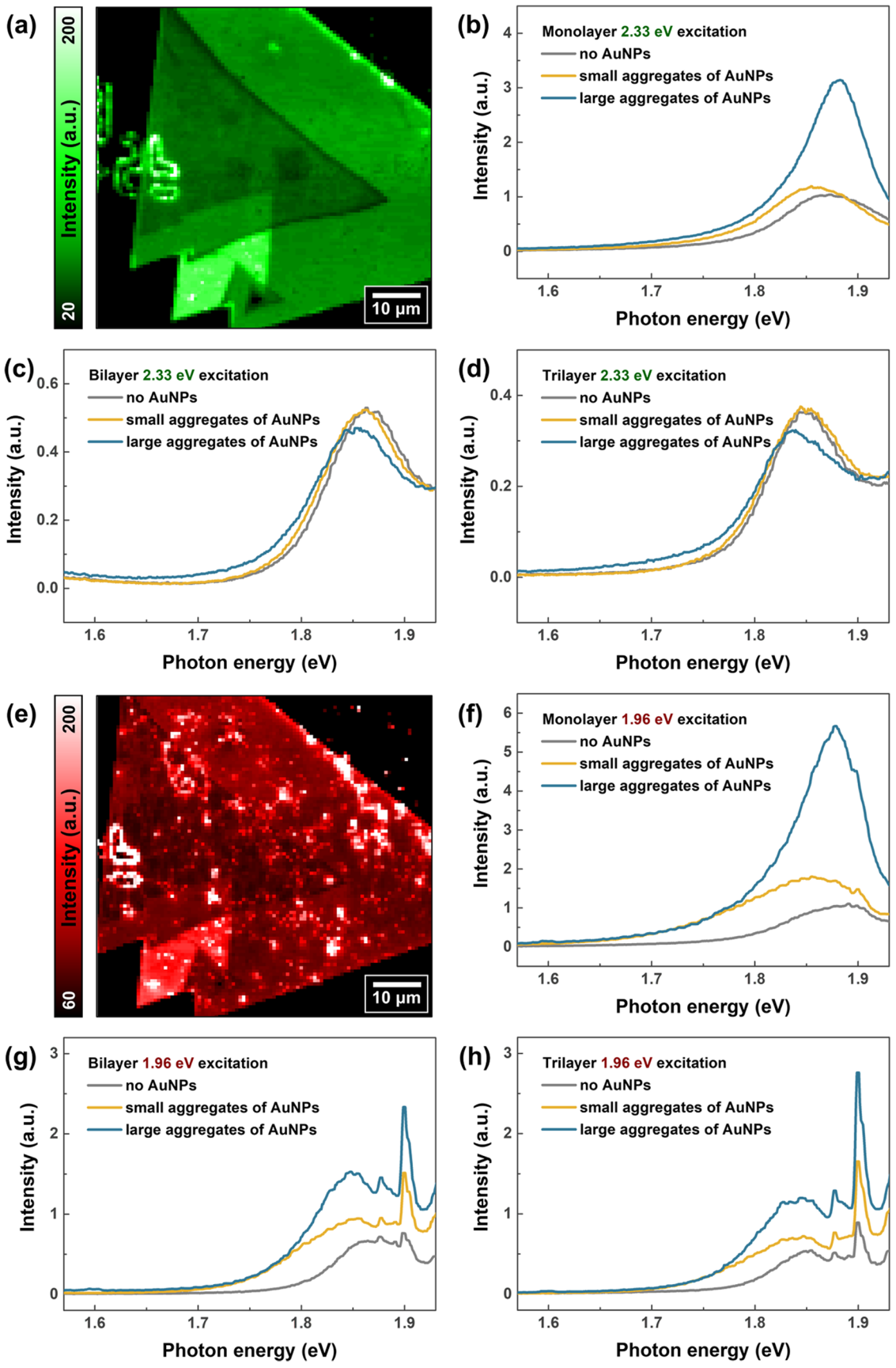

Figure 2. Photoluminescence (PL) of the MoS_2/AuNPs hybrid structure. (a) Integrated PL intensity image under nonresonant excitation at 2.33 eV. Nonresonance PL spectra of (b) 1L, (c) 2L, and (d) 3L MoS_2 depending on the size of AuNP aggregates. (e) Integrated PL intensity image under resonant excitation at 1.96 eV. Resonance PL spectra of (f) 1L, (g) 2L, and (h) 3L MoS_2 depending on the size of AuNP aggregates.

https://doi.org/10.1021/acsomega.4c02442
ACS Omega 2024, 9, 21587−21594

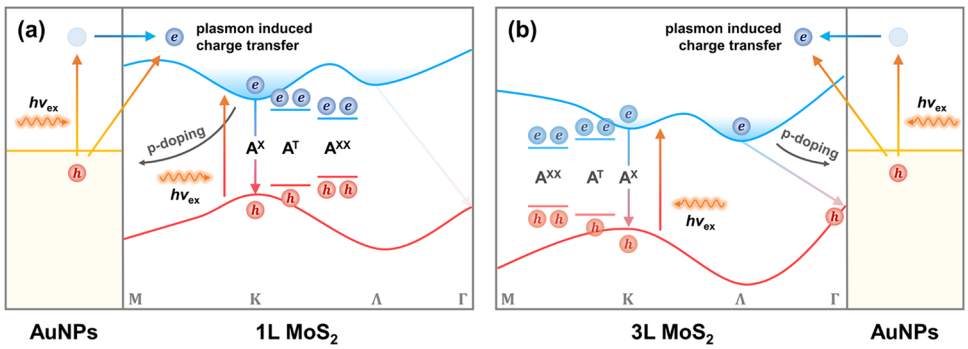

Figure 3. Electronic band structure of (a) 1L MoS_2/AuNPs and (b) 3L MoS_2/AuNPs. Because the A exciton emission occurs at the K-point, a pronounced doping effect is observed in 1L MoS_2, where the conduction band minimum is located at the K-point, but not in 3L MoS_2.

Figure 1b shows the optical reflectance spectra observed in MoS_2 and AuNPs. The SiO_2/Si substrate was used as a reference surface. In MoS_2, the reduction in reflection is attributed to absorption occurring at 1.90 and 2.04 eV, corresponding to the A and B excitonic emission energies, respectively. The spectrum observed in the ring-shaped AuNPs with a diameter of 100 nm exhibits a spectral dip spanning from 1.60 to 2.10 eV, with the center located at 1.85 eV. This spectral dip arises from the absorption caused by LSPR.

The change in the doping level of MoS_2 due to contact with AuNPs was investigated using Kelvin probe force microscopy (KPFM) as shown in Figure 1c. The contact potential difference (CPD) decreases as the number of layers increases in MoS_2 on the SiO_2/Si substrate. MoS_2/AuNPs exhibit a lower CPD compared to MoS_2, which indicates that the contact with AuNPs induces p-doping.[16,34−36] In particular, p-doping is observed in regions where strain is applied, leading to a weak doping effect in single AuNPs with a simple structure but a strong doping effect in large aggregates of AuNPs with a complex structure. This doping effect of MoS_2/AuNPs is most prominent in 1L rather than in 2L and 3L as presented in Figure 1d. This is because the potential difference between 1L MoS_2 and Au is larger than that between 2L or 3L MoS_2 and Au, and electrons can transfer more easily for lower layer numbers of MoS_2.[37]

AuNP Aggregate Size-Dependent Photoluminescence of MoS_2. Figure 2a illustrates the total PL intensity image of the MoS_2/AuNPs heterohybrid structures obtained by integrating over the spectral range from 1.57 to 1.93 eV under nonresonant excitation at 2.33 eV. It exhibits a decrease in PL intensity as the number of MoS_2 layers increases, enabling a clear distinction between MoS_2 layer numbers, while revealing almost no change in PL intensity associated with AuNPs except for 1L MoS_2. Enhanced PL is only prominent in 1L MoS_2/AuNPs (see Figure 2b) and the 3L MoS_2/Au-masked structure. Conversely, 2L and 3L MoS_2/AuNPs exhibit either the same or quenched PL, depending on the size of AuNP aggregates as shown in Figure 2c,d. The same process was performed under resonance excitation conditions. Figure 2e displays an image representing the integrated PL intensity under excitation at 1.96 eV. Because the energy of the exciting laser is close to the energy of an allowed electronic absorption, the resonance Raman spectrum is measured in the energy range of 1.87 eV and more, along with the PL spectrum; see the Supporting Information, Figure S2. In contrast to the case of nonresonant excitation, the 1.96 eV laser excites the LSPR, which enhances the PL intensity of MoS_2/AuNPs across all layers. Even in multilayers, higher enhancements, rather than quenching, are observed at large aggregates of AuNPs as shown in Figure 2f−2h. In addition to alterations in the PL intensity, changes in the peak position and spectral width are observed. In 1L MoS_2/AuNPs, a broader spectrum is observed at lower energy when the aggregates of AuNPs are small, while a sharper spectrum is seen at higher energy when the aggregates of AuNPs are large as presented in Figure 2b,f. However, even with large aggregates of AuNPs, the PL spectra of multilayer MoS_2/AuNPs exhibit emissions at lower energy as shown in Figure 2c,d,2g,2h.

The changes in the PL spectra of MoS_2/AuNPs are primarily influenced by strain, doping, and LSPR. Figure 3a depicts the schematic electronic band structure of 1L MoS_2/AuNPs. For smaller aggregates of AuNPs, it is difficult to expect spectral changes due to the low degree of p-doping of MoS_2. However, because the induced biaxial strain deforms the conduction band minimum at the *K*-point, a funnel effect occurs.[19,20] In particular, under LSPR excitation conditions, additional electrons and excitons are generated in MoS_2 by plasmon-induced charge transfer and field enhancement.[26−28] Because the funnel effect, extra charge, and excitons promote the formation of higher order charge complexes, higher PL emission at lower energies can be observed.[38,39] With large aggregates of AuNPs, MoS_2 experiences a substantial p-doping effect (see Figure 1d), resulting in a decrease in electron density and a reduction in band gap renormalization.[40,41] Moreover, the decrease in the electron density of MoS_2 reduces the electrical conductivity and associated reflectivity, consequently enhancing the PL intensity. The resultant PL exhibits no discernible blue shift when compared to the absence of AuNPs, attributed to a reduction in band gap energy caused by strain. Despite the increase in excitonic emission, there was no corresponding increase in the emission of higher order charge complexes by the funnel effect and LSPR.

Multilayer MoS_2 has an indirect band gap because its conduction band minimum is at the Λ (also denoted as Q or ∑) point, and its valence band maximum is at the Γ point as illustrated in Figure 3b. Because the electron density mainly decreases at the Λ point due to p-doping, there is no significant change in the electron density at the *K*-point, making it difficult to expect a noticeable variation in A exciton emission.[42] When electrons are excited by light, they preferentially occupy the Λ state, where a radiative indirect transition can occur, but a non-negligible portion transitions to the K state, leading to a radiative direct transition.[43] Under nonresonant excitation conditions, AuNPs induce p-doping in MoS_2, leading to quenching in PL emission that scales

https://doi.org/10.1021/acsomega.4c02442
ACS Omega 2024, 9, 21587−21594

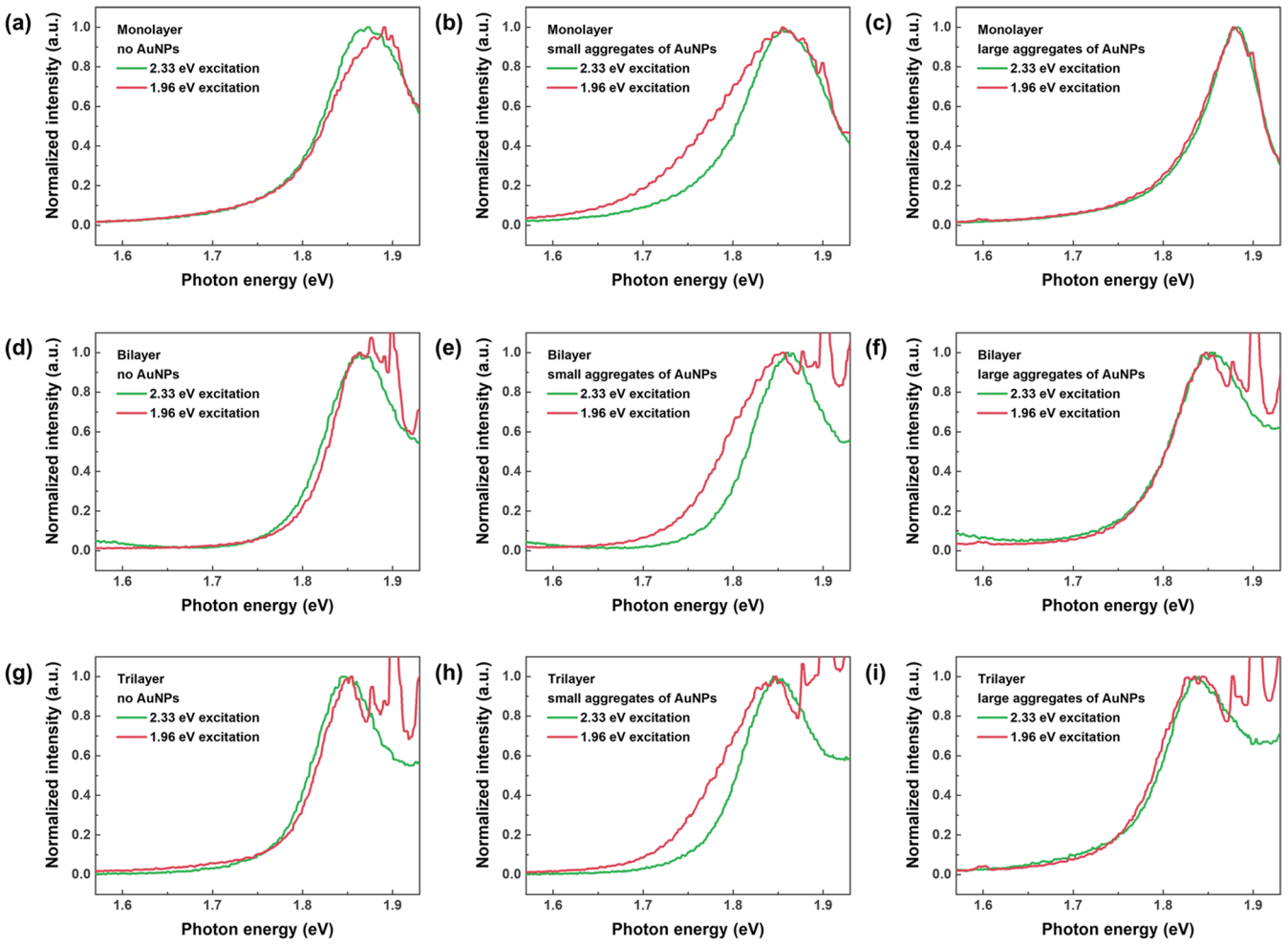

Figure 4. Nonresonance and resonance PL spectra of (a) 1L MoS_2, (b) 1L MoS_2 on small aggregates of AuNPs, (c) 1L MoS_2 on large aggregates of AuNPs, (d) 2L MoS_2, (e) 2L MoS_2 on small aggregates of AuNPs, (f) 2L MoS_2 on large aggregates of AuNPs, (g) 3L MoS_2, (h) 3L MoS_2 on small aggregates of AuNPs, and (i) 3L MoS_2 on large aggregates of AuNPs. Significant changes in the spectral shape are observed only in small aggregates of AuNPs.

proportionally with the size of AuNP aggregates. However, in the multilayer MoS_2/Au-masked structure, enhancement is observed rather than quenching. This is because of the PL of the Au sidewall at 1.95 eV; see the Supporting Information, Figure S3. Under resonant excitation conditions, despite the induced p-doping, the PL emission shows proportionality to the size of AuNP aggregates due to efficient light absorption and plasmon-induced charge transfer by AuNPs. Contrary to the blue shift of PL observed in 1L MoS_2/AuNPs resulting from substantial p-doping, multilayer MoS_2/AuNPs exhibit a red shift primarily attributed to strain because the alteration in charge density at the K-point due to doping is small.

Resonant and Nonresonant Excitation Effects in the Photoluminescence Spectral Shape. To analyze the PL spectral shape under different excitation conditions, normalized PL spectra for nonresonant and resonant excitations are plotted based on the number of MoS_2 layers and the size of AuNP aggregates, as shown in Figure 4. Interestingly, in the absence (see Figure 4a,4d,4g) or large aggregates (see Figure 4c,4f,4i) of AuNPs, little change in the spectral shape was observed, whereas in the small aggregates of AuNPs (see Figure 4b,e,4h), an increase in relative PL emission at lower energy was observed. These differences may occur due to local strain. The strain in MoS_2, induced by small aggregates of AuNPs, primarily originates from the height difference between the AuNPs and the substrate. Because of the small amount of AuNPs, the strain area is narrow, concentrating the funnel effect. In MoS_2 with large aggregates of AuNPs, additional strain can be induced by the height disparity among the AuNPs. In this scenario, while stronger strain may be induced, it results in a larger strain area and a dispersed funnel effect. The concentration of the funnel effect provides an opportunity for the extra charge or exciton to form more trions or biexcitons.

CONCLUSIONS

In conclusion, we analyzed the PL spectra of MoS_2/AuNPs, considering the layer number of MoS_2 and size of AuNP aggregates under both nonresonant and resonant excitation conditions. In 1L MoS_2/AuNPs, the PL intensity proportional to the size of AuNP aggregates was observed regardless of the excitation conditions. However, depending on the size of the aggregates, the peak shift showed an opposite tendency. In the case of small aggregates of AuNPs, a spectral red shift was observed, primarily resulting from induced strain, while in large aggregates, a blue shift was observed mainly due to p-doping. The changes in PL intensity of 2L and 3L MoS_2/AuNPs were different depending on the excitation conditions. As the size of

https://doi.org/10.1021/acsomega.4c02442
ACS Omega 2024, 9, 21587−21594

AuNP aggregates increases, the PL intensity was quenched mainly because of the p-doping, until a direct band gap is formed by strain in MoS_2 under nonresonant excitation conditions. On the other hand, under resonant excitation conditions, the PL intensity was enhanced by LSPR. Under resonant excitation conditions, the PL intensity experienced enhancement attributed to the heightened LSPR effect, directly correlated with the illuminated quantity of AuNPs. In all layers, distinct changes in the spectral shape based on excitation conditions were prominent solely in small aggregates of AuNPs. This is likely because localization by AuNPs becomes more pronounced in scenarios with fewer particles. Our results indicate the potential to manipulate the electrical and optical performance of the device by controlling the number of TMD layers and aggregate size of plasmonic nanoparticles. We believe that controlling and manipulating photoresponses through the TMDs and plasmonic nanoparticles, combined with a comprehensive understanding of these processes, will be instrumental in advancing the development of optoelectric and photonic devices.

MATERIALS AND METHODS

Synthesis of Au Nanorings. Au nanoprisms were employed as the initial materials for synthesizing gold nanorings. First, the vertices of Au nanoprisms were truncated to form thin gold nanodisks, with a height of approximately 10 ± 1 nm, using Au^{3+} ions as the etchant. Afterward, during the thickening step, the thin Au nanodisks evolved into Au nanohexagons by depositing Au. Subsequently, the Au nanohexagons were further etched into Au thick nanodisks with a height of approximately 25 ± 2 nm. In the selective edge deposition of Pt, Pt atoms were placed selectively at the periphery of thick Au nanodisks. This decoration is facilitated by the presence of high-index crystalline facets, which lower the activation energy barrier for Pt nucleation. In the next step, the core Au domains were etched by adding Au^{3+} ions, leading to the formation of Au@Pt split frames. Eventually, in the Au regrowth step, Au atoms were homogeneously reduced across the entire surface of split Pt nanorings, resulting in the formation of Au nanorings.[44]

MoS_2 Growth and Transfer Process. The synthesis of single-layer MoS_2 was achieved through a two-zone furnace chemical vapor deposition (CVD) process. The Mo precursor was prepared by mixing 0.008 M ammonium heptamolybdate (AHM, Sigma-Aldrich, 431346), 0.125 M NaOH, iodixanol (Sigma-Aldrich, Opti Prep, D1556), and deionized (DI) water in 0.3:2:0.2:1 volumetric ratio. The solution was then spread onto a SiO_2/Si substrate, which had been pretreated with oxygen plasma (30 W for 1 min), using a spin coater at 4000 rpm for 40 s.

The coated substrate, cut into a 1 × 1 cm^2 dimension, was placed in the downstream zone of a 2 in. tube furnace. Also, 200 mg of S (Sigma-Aldrich, no. 212392) was positioned in the upstream zone. For growth, the temperature of the downstream zone was modified to 190 °C, while the upstream zone was brought up to 780 °C. During this ramping period, which lasted for 12 min, a N_2 gas flow was maintained at 300 standard cubic centimeters per minute (sccm). This flow rate was then increased to 1000 sccm and maintained for an additional 7 min to facilitate the growth of the MoS_2. The entire process occurred at ambient pressure, and a purging step at the onset was determined to be unnecessary.

After the growth process, the MoS_2 layer was transferred by using the PMMA method. The MoS_2 was first coated with PMMA, spun at 4000 rpm for 40 s. It was then soaked in a 0.125 M NaOH solution to separate the MoS_2 layer from its growth substrate. Following this, it was rinsed with DI water to eliminate any NaOH residue. Finally, the PMMA/MoS_2 layer was transferred onto a SiO_2/Si substrate, which had been predeposited with gold nanoparticles followed by acetone and isopropyl alcohol (IPA) rinsing to remove the PMMA binder.

Sample Characterization. In optical characterization, the illumination source was focused on the sample via a 50× objective lens (Nikon, TU Plan Epi ELWD, NA 0.60). The reflected optical signal and photoluminescence (PL) were recorded and analyzed by a spectrometer (Princeton Instruments, SpectraPro 2300i, 150 lpmm) equipped with a CCD (Princeton Instruments, ProEM: 1600^2). For reflectance spectroscopy, a white LED was used as the light source. The exposure time of each spectrum was set to 100 ms. For PL spectroscopy, a 532 nm DPSS laser (Optoelectronicstech, MGLIII-532) and a 632.8 nm He−Ne laser (Thorlabs, HNL210LB) are utilized as nonresonant and resonant excitation sources, respectively. The excitation power was set to 200 μW after the objective lens, and the optical path was controlled by a 2D galvo mirror system (GVSM002, Thorlabs, Inc.) for 2D PL mapping.

In electrical characterization, Kelvin probe force microscopy was employed to measure the surface potential of MoS_2/AuNPs heterohybrid structures. The topographic and surface potential images were recorded simultaneously via commercial scanning probe microscopy (Parksystems, XE-NSOM) with an Au-coated cantilever (MikroMasch, NSC-14−Cr-Au). EFM (EXT) mode was used for the measurement, and the external lock-in amplifier (Stanford Research Systems, SR830) was set to a time constant of 300 μs, sensitivity of 5 mV, and AC voltage of 0.45 V. The scan was performed at a speed of 0.01 line/s over 60 μm × 60 μm (512 pxl × 512 pxl).

ASSOCIATED CONTENT

Supporting Information

The Supporting Information is available free of charge at https://pubs.acs.org/doi/10.1021/acsomega.4c02442.

Optical images of spectral test points, resonance Raman spectra of MoS_2, photoluminescence spectra of the gold-masked structures, and photoluminescence of MoS_2/AuNPs at different positions (PDF)

AUTHOR INFORMATION

Corresponding Author

Soobong Choi − *Department of Physics, Incheon National University, Incheon 22012, Republic of Korea;* orcid.org/0000-0003-4116-889X; Email: sbchoi@inu.ac.kr

Authors

Kiin Nam − *Department of Physics, Incheon National University, Incheon 22012, Republic of Korea;* orcid.org/0000-0001-6047-3131

Jaeseung Im − *Department of Physics, Incheon National University, Incheon 22012, Republic of Korea;* orcid.org/0000-0002-1291-2475

Gang Hee Han − *Department of Physics, Incheon National University, Incheon 22012, Republic of Korea;* orcid.org/0000-0003-2560-8170

https://doi.org/10.1021/acsomega.4c02442
ACS Omega 2024, 9, 21587−21594

Jin Young Park − *Department of Physics, Incheon National University, Incheon 22012, Republic of Korea*
Hyuntae Kim − *System Research & Development System Integration Team, Park Systems Corporation, Suwon 16229, Republic of Korea*
Sungho Park − *Department of Chemistry, Yonsei University, Seoul 03722, Republic of Korea;* orcid.org/0000-0001-5435-3125
Sungjae Yoo − *Biomaterials Research Center, Biomedical Research Division, Korea Institute of Science and Technology, Seoul 02792, Republic of Korea*
MohammadNavid Haddadnezhad − *Department of Chemistry, Sungkyunkwan University, Suwon 16419, Republic of Korea*
Jae Sung Ahn − *Medical & Bio Photonics Research Center, Korea Photonics Technology Institute, Gwangju 61007, Republic of Korea;* orcid.org/0000-0002-5107-0848
Kyoung-Duck Park − *Department of Physics, Pohang University of Science and Technology, Pohang 37673, Republic of Korea;* orcid.org/0000-0002-9302-9384

Complete contact information is available at: https://pubs.acs.org/10.1021/acsomega.4c02442

Notes

The authors declare no competing financial interest.

■ ACKNOWLEDGMENTS

This research was supported by the Commercialization Promotion Agency for R&D Outcomes (COMPA) and Nano & Material Technology Development Program through the National Research Foundation of Korea (NRF) funded by the Ministry of Science and ICT (MSIT) (1711198537 and NRF-2022M3H4A4085814). This research was also supported by the Industrial Strategic Technology Development Program funded by the Ministry of Trade, Industry & Energy (20017214 and 20019223). This research was also supported by the Technology development Program funded by the Ministry of SMEs and Startups (MSS) (RS-2023-00274278).

■ REFERENCES

(1) Lan, H. Y.; Hsieh, Y. H.; Chiao, Z. Y.; Jariwala, D.; Shih, M. H.; Yen, T. J.; Hess, O.; Lu, Y. J. Gate-Tunable Plasmon-Enhanced Photodetection in a Monolayer MoS_2 Phototransistor with Ultrahigh Photoresponsivity. *Nano Lett.* **2021**, *21* (7), 3083−3091.
(2) Le Thi, H. Y.; Ngo, T. D.; Phan, N. A. N.; Shin, H.; Uddin, I.; Venkatesan, A.; Liang, C. Te.; Aoki, N.; Yoo, W. J.; Watanabe, K.; Taniguchi, T.; Kim, G. H. Doping-Free High-Performance Photovoltaic Effect in a WSe_2 Lateral p-n Homojunction Formed by Contact Engineering. *ACS Appl. Mater. Interfaces* **2023**, *15* (29), 35342−35349.
(3) Najafidehaghani, E.; Gan, Z.; George, A.; Lehnert, T.; Quyet Ngo, G.; Neumann, C.; Bucher, T.; Staude, I.; Kaiser, D.; Vogl, T.; Hübner, U.; Kaiser, U.; Eilenberger, F.; Turchanin, A. 1D p−n Junction Electronic and Optoelectronic Devices from Transition Metal Dichalcogenide Lateral Heterostructures Grown by One-Pot Chemical Vapor. *Adv. Funct. Mater.* **2021**, *31* (27), No. 2101086.
(4) Bhatnagar, M.; Gardella, M.; Giordano, M. C.; Chowdhury, D.; Mennucci, C.; Mazzanti, A.; Valle, G. D.; Martella, C.; Tummala, P.; Lamperti, A.; Molle, A.; de Mongeot, F. B. Broadband and Tunable Light Harvesting in Nanorippled MoS_2 Ultrathin Films. *ACS Appl. Mater. Interfaces* **2021**, *13* (11), 13508−13516.
(5) Bucher, T.; Vaskin, A.; Mupparapu, R.; Löchner, F. J. F.; George, A.; Chong, K. E.; Fasold, S.; Neumann, C.; Choi, D. Y.; Eilenberger, F.; Setzpfandt, F.; Kivshar, Y. S.; Pertsch, T.; Turchanin, A.; Staude, I. Tailoring Photoluminescence from MoS_2 Monolayers by Mie-Resonant Metasurfaces. *ACS Photonics* **2019**, *6* (4), 1002−1009.
(6) Bernhardt, N.; Koshelev, K.; White, S. J. U.; Wong, K. W. C.; Frö, J. E.; Kim, S.; Tran, T. T.; Choi, D. Y.; Kivshar, Y.; Solntsev, A. S. Quasi-BIC Resonant Enhancement of Second-Harmonic Generation in WS_2 Monolayers. *Nano Lett.* **2020**, *20* (7), 5309−5314, DOI: 10.1021/acs.nanolett.0c01603.
(7) Löchner, F. J. F.; George, A.; Koshelev, K.; Bucher, T.; Najafidehaghani, E.; Fedotova, A.; Choi, D. Y.; Pertsch, T.; Staude, I.; Kivshar, Y.; Turchanin, A.; Setzpfandt, F. Hybrid Dielectric Metasurfaces for Enhancing Second-Harmonic Generation in Chemical Vapor Deposition Grown MoS_2 Monolayers. *ACS Photonics* **2021**, *8* (1), 218−227.
(8) Shen, F.; Zhang, Z.; Zhou, Y.; Ma, J.; Chen, K.; Chen, H.; Wang, S.; Xu, J.; Chen, Z. Transition Metal Dichalcogenide Metaphotonic and Self-Coupled Polaritonic Platform Grown by Chemical Vapor Deposition. *Nat. Commun.* **2022**, *13* (1), No. 5597.
(9) Alamri, M.; Gong, M.; Cook, B.; Goul, R.; Wu, J. Z. Plasmonic WS_2 Nanodiscs/Graphene van Der Waals Heterostructure Photodetectors. *ACS Appl. Mater. Interfaces* **2019**, *11* (36), 33390−33398.
(10) Cheng, F.; Johnson, A. D.; Tsai, Y.; Su, P. H.; Hu, S.; Ekerdt, J. G.; Shih, C. K. Enhanced Photoluminescence of Monolayer WS_2 on Ag Films and Nanowire-WS_2-Film Composites. *ACS Photonics* **2017**, *4* (6), 1421−1430.
(11) Lee, H.; Kim, I.; Park, C.; Kang, M.; Choi, J.; Jeong, K.-Y.; Mun, J.; Kim, Y.; Park, J.; Raschke, M. B.; Park, H. G.; Jeong, M. S.; Rho, J.; Park, K. D. Inducing and Probing Localized Excitons in Atomically Thin Semiconductors via Tip-enhanced Cavity-spectroscopy. *Adv. Funct. Mater.* **2021**, *31* (33), No. 2102893.
(12) Kwon, S.; Lee, S. Y.; Choi, S. H.; Kang, J. W.; Lee, T.; Song, J.; Lee, S. W.; Cho, C. H.; Kim, K. K.; Yee, K. J.; Kim, D. W. Polarization-Dependent Light Emission and Charge Creation in MoS_2 Monolayers on Plasmonic Au Nanogratings. *ACS Appl. Mater. Interfaces* **2020**, *12* (39), 44088−44093.
(13) Rahaman, M.; Rodriguez, R. D.; Plechinger, G.; Moras, S.; Schüller, C.; Korn, T.; Zahn, D. R. T. Highly Localized Strain in a MoS_2/Au Heterostructure Revealed by Tip-Enhanced Raman Spectroscopy. *Nano Lett.* **2017**, *17* (10), 6027−6033.
(14) Cuadra, J.; Baranov, D. G.; Wersäll, M.; Verre, R.; Antosiewicz, T. J.; Shegai, T. Observation of Tunable Charged Exciton Polaritons in Hybrid Monolayer WS_2-Plasmonic Nanoantenna System. *Nano Lett.* **2018**, *18* (3), 1777−1785.
(15) Lin, J.; Li, H.; Zhang, H.; Chen, W. Plasmonic Enhancement of Photocurrent in MoS_2 Field-Effect-Transistor. *Appl. Phys. Lett.* **2013**, *102* (20), No. 203109.
(16) Kim, H.; Im, J.; Nam, K.; Han, G. H.; Park, J. Y.; Yoo, S.; Haddadnezhad, M.; Park, S.; Park, W.; Ahn, J. S.; Park, D.; Jeong, M. S.; Choi, S. Plasmon-Exciton Couplings in the MoS_2/AuNP Plasmonic Hybrid Structure. *Sci. Rep.* **2022**, *12* (1), No. 22252.
(17) Luong, D. H.; Lee, H. S.; Ghimire, G.; Lee, J.; Kim, H.; Yun, S. J.; An, G. H.; Lee, Y. H. Enhanced Light−Matter Interactions in Self-Assembled Plasmonic Nanoparticles on 2D Semiconductors. *Small* **2018**, *14* (47), No. 1802949.
(18) Lloyd, D.; Liu, X.; Christopher, J. W.; Cantley, L.; Wadehra, A.; Kim, B. L.; Goldberg, B. B.; Swan, A. K.; Bunch, J. S. Band Gap Engineering with Ultralarge Biaxial Strains in Suspended Monolayer MoS_2. *Nano Lett.* **2016**, *16* (9), 5836−5841.
(19) Koo, Y.; Kim, Y.; Choi, S. H.; Lee, H.; Choi, J.; Lee, D. Y.; Kang, M.; Lee, H. S.; Kim, K. K.; Lee, G.; Park, K. D. Tip-Induced Nano-Engineering of Strain, Bandgap, and Exciton Funneling in 2D Semiconductors. *Adv. Mater.* **2021**, *33* (17), No. 2008234.
(20) Guo, Y.; Li, B.; Huang, Y.; Du, S.; Sun, C.; Luo, H.; Liu, B.; Zhou, X.; Yang, J.; Li, J.; Gu, C. Direct Bandgap Engineering with Local Biaxial Strain in Few-Layer MoS_2 Bubbles. *Nano Res.* **2020**, *13* (8), 2072−2078.
(21) Choi, M. Strain-Enhanced p Doping in Monolayer MoS_2. *Phys. Rev. Appl.* **2018**, *9* (2), No. 024009.
(22) Brumme, T.; Calandra, M.; Mauri, F. First-Principles Theory of Field-Effect Doping in Transition-Metal Dichalcogenides: Structural

Properties, Electronic Structure, Hall Coefficient, and Electrical Conductivity. *Phys. Rev. B* **2015**, *91* (15), No. 155436, DOI: 10.1103/PhysRevB.91.155436.
(23) Mak, K. F.; He, K.; Lee, C.; Lee, G. H.; Hone, J.; Heinz, T. F.; Shan, J. Tightly Bound Trions in Monolayer MoS_2. *Nat. Mater.* **2013**, *12* (3), 207−211.
(24) Finkelstein, G.; Shtrikman, H.; Bar-Joseph, I. Optical Spectroscopy of a Two-Dimensional Electron Gas near the Metal-Insulator Transition. *Phys. Rev. Lett.* **1995**, *74* (6), 976−979.
(25) Mouri, S.; Miyauchi, Y.; Matsuda, K. Tunable Photoluminescence of Monolayer MoS_2 via Chemical Doping. *Nano Lett.* **2013**, *13* (12), 5944−5948.
(26) Brongersma, M. L.; Halas, N. J.; Nordlander, P. Plasmon-Induced Hot Carrier Science and Technology. *Nat. Nanotechnol.* **2015**, *10* (1), 25−34.
(27) Wen, X.; Chen, S.; Zhao, J.; Du, W.; Zhao, W. Enhanced Plasmonic Hot-Carrier Transfer in Au/WS_2 Heterojunctions under Nonequilibrium Condition. *ACS Photonics* **2022**, *9* (5), 1522−1528.
(28) Ratchford, D. C. Plasmon-Induced Charge Transfer: Challenges and Outlook. *ACS Nano* **2019**, *13* (12), 13610−13614.
(29) Puchert, R. P.; Steiner, F.; Plechinger, G.; Hofmann, F. J.; Caspers, I.; Kirschner, J.; Nagler, P.; Chernikov, A.; Schüller, C.; Korn, T.; Vogelsang, J.; Bange, S.; Lupton, J. M. Spectral Focusing of Broadband Silver Electroluminescence in Nanoscopic FRET-LEDs. *Nat. Nanotechnol.* **2017**, *12* (7), 637−641.
(30) Sriram, P.; Wen, Y. P.; Manikandan, A.; Hsu, K. C.; Tang, S. Y.; Hsu, B. W.; Chen, Y. Z.; Lin, H. W.; Jeng, H. T.; Chueh, Y. L.; Yen, T. J. Enhancing Quantum Yield in Strained MoS_2 Bilayers by Morphology-Controlled Plasmonic Nanostructures toward Superior Photodetectors. *Chem. Mater.* **2020**, *32* (6), 2242−2252.
(31) Sun, N.; Chen, Z.; Huang, J.; Liu, X.; Hu, T.; Zhao, P.; Zhang, Z.; Liu, X.; Xie, Y.; Liu, Q. Large-Scale Manipulation of Monolayer MoS_2 Photoluminescence via Size-Tunable Plasmonic Nanoparticles: Implications for Information Encoding and Optical Anti-Counterfeiting. *ACS Appl. Nano Mater.* **2023**, *6* (18), 17285−17293.
(32) Sriram, P.; Wen, Y. P.; Manikandan, A.; Hsu, K. C.; Tang, S. Y.; Hsu, B. W.; Chen, Y. Z.; Lin, H. W.; Jeng, H. T.; Chueh, Y. L.; Yen, T. J. Enhancing quantum yield in strained MoS_2 bilayers by morphology-controlled plasmonic nanostructures toward superior photodetectors. *Chem. Mater.* **2020**, *32* (6), 2242−2252.
(33) Garai, M.; Zhu, Z.; Shi, J.; Li, S.; Xu, Q. H. Single-particle studies on plasmon enhanced photoluminescence of monolayer MoS_2 by gold nanoparticles of different shapes. *J. Chem. Phys.* **2021**, *155* (23), No. 234201.
(34) Bhanu, U.; Islam, M. R.; Tetard, L.; Khondaker, S. I. Photoluminescence quenching in gold - MoS_2 hybrid nanoflakes. *Sci. Rep.* **2014**, *4* (1), No. 5575.
(35) Tugchin, B. N.; Doolaard, N.; Barreda, A. I.; Zhang, Z.; Romashkina, A.; Fasold, S.; Staude, I.; Eilenberger, F.; Pertsch, T. Photoluminescence Enhancement of Monolayer WS_2 by n-Doping with an Optically Excited Gold Disk. *Nano Lett.* **2023**, *23* (23), 10848−10855.
(36) Yan, J.; Ma, C.; Liu, P.; Yang, G. Plasmon-induced energy transfer and photoluminescence manipulation in MoS_2 with a different number of layers. *ACS Photonics* **2017**, *4* (5), 1092−1100.
(37) Sohn, A.; Moon, H.; Kim, J.; Seo, M.; Min, K. A.; Lee, S. W.; Yoon, S.; Hong, S.; Kim, D. W. Band Alignment at Au/MoS_2 Contacts: Thickness Dependence of Exfoliated Flakes. *J. Phys. Chem. C* **2017**, *121* (40), 22517−22522.
(38) Lee, H.; Koo, Y.; Choi, J.; Kumar, S.; Lee, H.; Ji, G.; Choi, S. H.; Kang, M.; Kim, K. K.; Park, H.; Choo, H.; Park, K. Drift-dominant exciton funneling and trion conversion in 2D semiconductors on the nanogap. *Sci. Adv.* **2022**, *8* (5), No. eabm5236.
(39) Chen, Z.; Luo, W.; Liang, L.; Ling, X.; Swan, A. K. Charge Separation in Monolayer WSe2 by Strain Engineering: Implications for Strain-Induced Diode Action. *ACS Appl. Nano Mater.* **2022**, *5* (10), 15095−15101.
(40) Gao, S.; Liang, Y.; Spataru, C. D.; Yang, L. Dynamical Excitonic Effects in Doped Two-Dimensional Semiconductors. *Nano Lett.* **2016**, *16* (9), 5568−5573.
(41) Raja, A.; Chaves, A.; Yu, J.; Arefe, G.; Hill, H. M.; Rigosi, A. F.; Berkelbach, T. C.; Nagler, P.; Schüller, C.; Korn, T.; Nuckolls, C.; Hone, J.; Brus, L. E.; Heinz, T. F.; Reichman, D. R.; Chernikov, A. Coulomb Engineering of the Bandgap and Excitons in Two-Dimensional Materials. *Nat. Commun.* **2017**, *8* (1), No. 15251.
(42) Pei, J.; Yang, J.; Xu, R.; Zeng, Y. H.; Myint, W.; Zhang, S.; Zheng, J. C.; Qin, Q.; Wang, X.; Jiang, W.; Lu, Y. Exciton and Trion Dynamics in Bilayer MoS_2. *Small* **2015**, *11* (48), 6384−6390.
(43) Kozawa, D.; Kumar, R.; Carvalho, A.; Amara, K. K.; Zhao, W.; Wang, S.; Toh, M.; Ribeiro, R. M.; Neto, A. H. C.; Matsuda, K.; Eda, G. Photocarrier Relaxation Pathway in Two-Dimensional Semiconducting Transition Metal Dichalcogenides. *Nat. Commun.* **2014**, *5* (1), No. 4543.
(44) Haddadnezhad, M.; Yoo, S.; Kim, J.; Kim, J. M.; Son, J.; Jeong, H. S.; Park, D.; Nam, J.; Park, S. Synthesis and Surface Plasmonic Characterization of Asymmetric Au Split Nanorings. *Nano Lett.* **2020**, *20* (10), 7774−7782.

https://doi.org/10.1021/acsomega.4c02442
ACS Omega 2024, 9, 21587−21594